Experimental invalidation of phase-transition-induced elastic softening in CrN

Shanmin Wang, Xiaohui Yu, Jianzhong Zhang, Miao Chen, Jinlong Zhu, Liping Wang, Duanwei He, Zhijun Lin, Ruifeng Zhang, Kurt Leinenweber, and Yusheng Zhao

Phys. Rev. B **86**, 064111 — Published 28 August 2012

DOI: 10.1103/PhysRevB.86.064111

Experimental invalidation of phase-transition induced elastic softening in CrN

Shanmin Wang,[1,2] Xiaohui Yu,[2] Jianzhong Zhang,[2] Miao Chen,[1] Jinlong Zhu,[2] Liping Wang,[3] Duanwei He,[1,*] Zhijun Lin,[2] Ruifeng Zhang,[4] Kurt Leinenweber,[5] and Yusheng Zhao[2,3,*]

[1]*Institute of Atomic & Molecular Physics, Sichuan University, Chengdu 610065, P. R. China*

[2]*LANSCE Division, Los Alamos National Laboratory, Los Alamos, NM 87545, USA*

[3]*HiPSEC, University of Nevada, Las Vegas, Nevada 89154, USA*

[4]*Theoretical Division, Los Alamos National Laboratory, Los Alamos, NM 87545, USA*

[5]*Deptartment of Chemistry and Biochemistry, Arizona State University, Tempe, AZ 85287, USA*

*** Corresponding authors:**

E-mail addresses: duanweihe@scu.edu.cn (D. He); Yusheng.Zhao@unlv.edu (Y. Zhao)

ABSTRACT

We report experimental results of phase stability and incompressibility of CrN. The obtained bulk moduli for cubic and orthorhombic CrN are 257 GPa and 262 GPa, respectively. These results invalidate the conclusion of phase-transition induced elastic softening recently reported based on nonmagnetic simulations for cubic CrN [*Nature Mater. 8, 947 (2009)*]. On the other hand, they provide the only experimental evidence to support the computational models involving local magnetic moment of Cr atoms *[Nature Mater. 9, 283 (2010)]*, indicating that atomic spin has profound influence on the material's elastic properties. We also demonstrate that nonstoichiometry in CrN_x has strong effects on its structural stability.

I. INTRODUCTION

Among transition-metal nitrides, chromium nitride (CrN) exhibits fascinating structural, magnetic, and electronic properties that are of fundamental importance to condensed-matter and computational physics.[1-5] At atmospheric pressure, CrN possesses an orthorhombic (*orthor*) structure and a unique antiferromagnetic ordering below the Neél temperature (T_N) of 286 K; it transforms into a cubic (*c*), paramagnetic configuration above T_N.[1] Recent studies on CrN provide new insights into structural transition that is driven by magnetic ordering.[2] The magnetic moment also plays crucial roles in a variety of physical phenomena in other material systems. For example, Mott transition in MnO[6] and elastic hardening in (Fe_x, Mg_{1-x})O[7] are commonly attributed to the collapse of magnetic moment under high pressure conditions. However, first-principles calculations for paramagnetic materials are typically performed without considering local magnetic moments associated with atomic spin. As a

result, the calculations for paramagnetic materials are often inconsistent with experimental observations. The experimentally reported bulk moduli for paramagnetic *c*-CoO and *c*-$PbCrO_3$, for example, are 180 GPa and 59 GPa, respectively, which are 70 % and 290 % lower than calculated values of 307 GPa and 230 GPa using nonmagnetic simulation.[8,9] Conflicting electronic properties have also been predicted for cubic, paramagnetic CrN by first-principles calculations, including metal, semiconductor, or insulator.[2, 4, 5]

The impacts of magnetostructural phase transition on elastic properties and electrical conductivity have recently been subjects of intense research for a wide range of materials including CrN,[2,10,11] TiN,[12] MnO,[6] Fe_2O_3,[13] $Fe_xMg_{1-x}O$,[7] $Fe_xMg_{1-x}SiO_3$,[14,15] and $PbCrO_3$.[9] In particular, *Rivadulla et al.* reported unprecedented elastic softening in CrN with the bulk modulus, B_0, of the high-pressure orthorhombic phase that is 25% smaller than that of low-pressure cubic phase.[10] Because these authors were unable to experimentally determine B_0 for the *c*-CrN due to its limited structural stability (i.e., stable only up to 1 GPa), their conclusion was mainly based on first-principles calculations that predicted a high B_0 of 340 GPa using a nonmagnetic model.[10] The computational scheme applied in Ref. **10**, however, was critically questioned by *Alling et al. (2010)* who obtained a substantially lower value of B_0 = 252 GPa when the local magnetic moment was introduced into the simulation package for the paramagnetic/cubic phase.[11] To date, the controversy between theories has yet been resolved,[16] calling for more rigorous experimental elucidation of this intriguing phenomenon. Here we report experimental results of incompressibility and phase stability of CrN based on high-pressure (P) synchrotron x-ray and time-of-flight neutron diffraction and electrical resistivity measurements at low temperatures (T).

II. EXPERIMENTAL DETAILS

Stoichiometric CrN was prepared by solid-state ion-exchange reaction between $NaCrO_2$ and *h*BN at 5 GPa and 1,573 K for 20 min, which is given by

$$NaCrO_2 + BN = CrN + NaBO_2 \qquad (1).$$

The unwanted byproduct $NaBO_2$ can be readily removed by washing the reaction product in water, leading to nearly phase-pure *c*-CrN. The experimental details can be found in Ref. **17**. Using similar reaction routes, we also successfully prepared nitrogen-rich tungsten nitrides (W_2N_3) and molybdenum nitrides (MoN_2),[18] indicating that our formulated solid-state ion-exchange reaction is an effective route to synthesize nitrogen-rich nitrides.

The experimental run products were characterized by x-ray diffraction (XRD) and time-of-flight neutron diffraction. Rietveld refinements were performed by using GSAS software.[10, 19] X-ray photoelectron spectroscopy (XPS) was used to determine stoichiometric composition. The Cr:N molar ratio is very close to 1:1 for the sample prepared by reaction (1). The sample density was determined using the Archimedes method on the bulk CrN samples sintered at 8 GPa and 2,073-2,273 K for 45 min. The measured densities are typically within 95% of the x-ray density. The sintered samples were characterized by x-ray diffraction; all final products for *c*-CrN are well-crystallized and nearly phase-pure. These combined characterizations indicate that our high-*P* synthetic route presents significant advantages over traditional synthetic methods.[10, 20]

Low-temperature electrical resistivity measurements were performed at ambient pressure on well-sintered CrN. The mirror-quality surfaces were prepared for the four-point electrical measurement. Compression experiments on CrN were conducted at pressures up to 40 GPa

and temperatures in the range of 300-1,200 K, using angular- and energy-dispersive synchrotron x-ray diffraction and time-of-flight neutron scattering. We used a diamond-anvil cell (DAC) for angular-dispersive experiments performed at the HPCAT 16BM-D beamline of Argonne National Laboratory. Neon was served as pressure-transmitting medium. Several ruby crystals were mounted inside the gasket hole to serve as internal pressure standards. Experimental details can be found elsewhere.[9] For energy-dispersive experiments, we used a DIA-type large-volume high-pressure apparatus installed at X17B2 beamline of the National Synchrotron Light Source, Brookhaven National Laboratory. The experimental details of this study are similar to those described in ref. **21**. We first compressed the pressure cell at room temperature to 8.7 GPa, followed by heating to the maximum temperature of 1,200 K, and subsequent cooling to 1,000 K, 800 K, 600 K, 400 K, and 300 K, respectively. XRD diffraction data were collected on cooling to minimize non-hydrostatic stress built up during the room temperature compression. The same procedures were repeated at progressively lower pressures. High *P*-*T* neutron scattering experiments were performed in a TAP-98 toroidal-anvil press at Lujan Neutron Scattering Center, Los Alamos Neutron Science Center.[22] In the latter two types of the experiments NaCl was used as internal pressure standard with pressures calculated using a Decker scale.[23]

III. RESULTS AND DISCUSSION

Fig. 1 shows XRD patterns collected at ambient conditions and at 11.3 GPa. The refined ambient lattice parameter for *c*-CrN is a = 4.1513 (2) Å, which is 0.08% larger than reported by *Rivadulla et al.* (4.1480 Å) for the sample synthesized by ammonolysis of Cr_3S_4.[10] To understand this small but conceivably meaningful difference, we subjected the high-*P*

synthesized CrN to a high-*T* treatment at 1,473 K for 1 hour in an Ar atmosphere. To our delight, we recovered a CrN sample with a = 4.1481 Å; quite obviously, the observed reduction in the lattice parameter can be attributed to nitrogen degassing at elevated temperature. Based on this finding, we infer that the sample synthesized by *Rivadulla et al. (2009)* is nitrogen-deficient with $x < 1$ in CrN_x.[10] At 11.3 GPa, the lattice parameters are a=5.684 Å, b=2.937 Å, and c=4.082 Å, corresponding to an x-ray density of 6.433 g/cm^3 [Fig. 1(b)]. The refined atomic positions are given below,

Cr: (x,1/4, z), Wyckoff site *4c,* x=0.1135*,* and z=1/4;

N: (x, 1/4, z), Wyckoff site *4c*, x=0.1155, and z=3/4.

Our refined x positions for Cr and N are different from those of *Croliss et al.*[1] who proposed x=1/8 for both Cr and N. However, because (200) and (211) peaks are observed in our XRD pattern, Cr and N should have different x values.

Fig. 2(a) shows typical angular-dispersive x-ray diffraction (XRD) patterns collected at room temperature in a DAC experiment. The onset pressure for the cubic-orthorhombic phase transition was determined to be ~4.9 GPa with the two CrN phases coexisted up to ~7.5 GPa. Consistent with these findings, we observed the cubic-to-orthorhombic phase transition at 5.3 (4) GPa in high *P-T* energy-dispersive synchrotron experiments using a large-volume apparatus. We also conducted high-pressure neutron diffraction experiments on CrN; at pressures up to 2.0 GPa, neither structural phase transition nor magnetic transition to an anti-ferromagnetic phase was observed at room temperature. These observations are markedly different from the commonly accepted value of 1 GPa for the cubic-to-orthorhombic phase transition in CrN.[10, 11] To further map out the phase boundary

for CrN, we carefully monitored the orthorhombic-cubic transition above room temperature. Shown in Fig. 2(b) and (c) are XRD patterns collected at selected high *P*-*T* conditions. Based on these observations, the transition pressures are determined to be 5.46 GPa at 315 K and 8.87 GPa at 358 K.

The low-*T* electrical resistivity measurements on well-sintered CrN show an abrupt drop near 240 K at atmospheric pressure [inset in Fig. 2(d)], which corresponds to the cubic-to-orthorhombic phase transition. Both of two phases are intrinsic metals, indicating that previously reported conflicts in electronic properties may be associated with crystalline disorders. The detailed discussion of these observations will be published elsewhere. This temperature is substantially lower than previously reported values of ~270 – 286 K for CrN samples prepared by traditional synthetic routes.[1,24,25] As pointed out by *Filippetti et al.*, nitrogen has a strong tendency to form dimmers, which leads to difficulties in growing defect-free transition-metal nitrides using those approaches.[3] We also show earlier that the CrN samples used in previous studies (e.g., Ref. **10**) are indeed nitrogen-deficient with $x < 1$ in CrN_x. These observations indicate that the Neel temperature in CrN_x may be sensitive to the degree of nonstoichiomerty. On the other hand, as illustrated in Fig. 2(d), the determined transition temperature of 240 (3) K at ambient pressure lines up very well with the transition points observed under high *P*-*T* conditions, allowing the phase boundary to be tightly constrained for stoichiometric CrN. Also plotted in Fig. 2(d) is the phase boundary derived from the results of *Rivadulla et al.* for nonstoichiometric CrN_x ($x < 1$),[10] indicating that the presence of crystal defects promotes the transition to substantially lower pressures. Further experimental and computational work is warranted to quantify and understand this effect. A

particular area of focus in the experimental studies is the stoichiometric composition of CrN_x, which needs to be accurately determined and reported in future publications.

The extended structural stability observed in this work for stoichiometric *c*-CrN allows the bulk modulus to be determined more accurately based on the pressure-volume measurements, which are illustrated in Fig. 3. The B_0 values derived from the DAC data using a Birch-Murnaghan equation of state[26] are 253 (12) GPa for *c*-CrN and 262 (6) GPa for *orthor*-CrN [Fig. 3(a)]. The relatively low B_0 in *c*-CrN is further confirmed by our robust high *P*-*T* synchrotron data, which lead to a more accurate value of B_0 = 257 (5) GPa [Fig. 3(b)]. The temperature derivative of B_0, $(\partial B_0/\partial T)_P$, was determined for the first time for the *c*-CrN and is found to be -2.95×10^{-2} GPa / K [Inset in Fig. 3(b)]. In addition, the B_0 derived from our experiments for *orthor*-CrN is in excellent agreement with the reported values in Refs. **10** and **11**. These experimental findings support the computational model of *Alling et al.*,[11] indicating that atomic spin has profound influence on the material's elastic properties. Our results, however, do not reveal any phase-transition induced elastic softening in CrN and hence invalidate the main conclusion and associated physical mechanisms reported by *Rivadulla et al.*.[10] Conceivably, the controversies between experiments and non-magnetic simulations for other paramagnetic materials CoO[8] and $PbCrO_3$[9] may also be resolved by computational models involving local magnetic moment. Further computational efforts along this direction are required to establish the ubiquity of this phenomenon for the family of paramagnetic materials. We conclude that CrN may show complex structural, elastic, and magnetic behaviors depending on the sample preparation procedure and defect chemistry.

ACKNOWLEDGMENTS

This work has partly benefited from the use of the Lujan Neutron Scattering Center at Los Alamos Neutron Science Center, which is funded by the U.S. Department of Energy's Office of Basic Energy Sciences. This work is also supported by the China 973 Program (Grant No. 2011CB808205), and the National Natural Science Foundation of China (Grant Nos. 11027405). We would thank Prof. Jianshi Zhou (*The University of Texas, Austin*) for low-temperature electrical resistivity measurements. The use of HPCAT (at 16BM-D beamline), APS is supported by Carnegie Institute of Washington, Carnegie DOE Alliance Center, University of Nevada at Las Vegas, and Lawrence Livermore National Laboratory through funding from DOE–National Nuclear Security Administration, DOE–Basic Energy Sciences, and NSF; APS is supported by DOE-BES, under Contract No. DE-AC02-06CH11357. Use of the National Synchrotron Light Source (at X17B2 beamline), Brookhaven National Laboratory, was supported by the U.S. Department of Energy, Office of Science, Office of Basic Energy Sciences, under Contract No. DE-AC02-98CH10886.

References:

[1]L. M. Corliss, N. Elliott, and J. M. Hastings, Phys. Rev. **117**, 929 (1960).

[2]A. Filippetti and N. A. Hill, Phys. Rev. Lett. **85**, 5166 (2000).

[3]A. Filippetti, W. E. Pickett, and B. M. Klein, Phys. Rev. B **59**, 7043 (1999).

[4]A. Herwadkar and W. R. L. Lambrecht, Rhys. Rev. B **79**, 10 (2009).

[5]B. Alling, T. Marten, and I. A. Abrikosov, Phys. Rev. B **82**, 184430 (2010).

[6]J. Kunes, A. V. Lukoyanov, V. I. Anisimov, R. T. Scalettar, and W. E. Pickett, Nature Mater. **7**, 198 (2008).

[7]J. F. Lin, V. V. Struzhkin, S. D. Jacobsen, M. Y. Hu, P. Chow, J. Kung, H. Z. Liu, H. K. Mao, and R. J. Hemley, Nature **436**, 377 (2005).

[8]J. F. Liu, Y. He, W. Chen, G. Q. Zhang, Y. W. Zeng, T. Kikegawa, and J. Z. Jiang, J. Phys. Chem. C **111**, 2 (2007).

[9]W. Xiao, D. Tan, X. Xiong, J. Liu, and J. Xu, Proc. Natl. Acad. Sci. USA **107**, 14026 (2010).

[10]F. Rivadulla, et al., Nature Mater. **8**, 947 (2009).

[11]B. Alling, T. Marten, and I. A. Abrikosov, Nature Mater. **9**, 283 (2010).

[12]V. M. Vinokur, T. I. Baturina, M. V. Fistul, A. Y. Mironov, M. R. Baklanov, and C. Strunk, Nature **452**, 613 (2008).

[13]S.-H. Shim, A. Bengtson, D. Morgan, W. Sturhahn, K. Cataiii, J. Zhao, M. Lerche, and V. Prakapenka, Proc. Natl. Acad. Sci. USA **106**, 5508 (2009).

[14]J.-F. Lin, et al., Nature Geosci. **1**, 688 (2008).

[15]T. Yamanaka, K. Hirose, W. L. Mao, Y. Meng, P. Ganesh, L. Shulenburger, G. Shen, and R. J. Hemley, Proc. Natl. Acad. Sci. USA **109**, 1035 (2012).

[16]F. Rivadulla, et al., Nature Mater. **9**, 284 (2010).

[17]M. Chen, S. M. Wang, J. Z. Zhang, D. W. He, and Y. S. Zhao, in submission (2012).

[18]S. M. Wang, in submission (2012).

[19]B. H. Toby, J. Appl. Cryst. **34**, 210 (2001).

[20]P. A. Bhobe, et al., Phys. Rev. Lett. **104**, 236404 (2010).

[21]J. Z. Zhang and P. J. Kostak, Phys. Earth Planet In. **129** (2002).

[22]Y. S. Zhao, R. B. von Dreele, and J. G. Morgan, High Pressure Res. **16**, 161 (1999).

[23]D. L. Decker, J. Appl. Phys. **42**, 3239 (1971).

[24]J. D. Browne, P. R. Liddell, R. Street, and T. Mills, Phys. State. Sol. (a) **1**, 715 (1970).

[25]D. Gall, C. S. Shin, R. T. Haasch, I. Petrov, and J. E. Greene, J. Appl. Phys. **91**, 5882 (2002).

[26]F. Birch, Phys. Rev. **71**, 809 (1947).

Figures and Captions:

FIG. 1 (Color online) Refined XRD patterns for CrN. **(a)** Ambient pressure pattern of *c*-CrN was collected with a copper target ($\lambda_{K\alpha 1}$ = 1.54056 Å and $\lambda_{K\alpha 2}$=1.54440 Å). **(b)** Synchrotron XRD pattern for *orthor*-CrN collected at 11.3 GPa with a wavelength of 0.40662 Å. Black circles and red lines denote the observed and calculated profiles, respectively. The difference curve between the observed and calculated profiles is shown in cyan color (below). The blue tick marks correspond to the peak positions.

FIG. 2 (Color online) Phase stability determined based on compression experiments and low-*T* electrical resistivity measurements. **(a)** Selected high-*P* angular-dispersive synchrotron XRD patterns collected in DAC at room temperature. The wavelength is 0.40662 Å. **(b)** and **(c)** Energy-dispersive synchrotron x-ray diffraction patterns at selected *P*-*T* conditions. At 315 K, *orthor*-to-*cubic* transition happens at 5.46 GPa; the transition pressure increases to 8.87 GPa at ~358 K. Fluorescence peaks of Pb and Cr are denoted as blue diamonds and blue dots, respectively. **(d)** The orthorhombic-cubic phase transition boundary determined by high *P*-*T* synchrotron XRD and low-*T* electrical resistivity measurements. Inset shows the electrical resistivity as a function of temperature. Phase transition happens at 240 (3) K.

FIG. 3 (Color online) Results of compression experiments. **(a)** Volume-pressure data of

cubic- (open pink squares) and *orthorhombic*-CrN (solid blue circles) collected at room temperature using angular-dispersive high-*P* synchrotron XRD in a DAC. Inset is an enlarged portion of data for *c*-CrN. Solid black circles represents the data obtained from high-*P* neutron diffraction experiments (0 – 2 GPa). **(b)** Isothermal volume-pressure data collected using energy-dispersive synchrotron XRD in a large-volume apparatus. Inset presents the isothermal bulk modulus as a function of temperature. All volume-pressure data fitted to the third-order Birch-Murnaghan equation of state with fixed $B'=4$[26].

FIG. 1

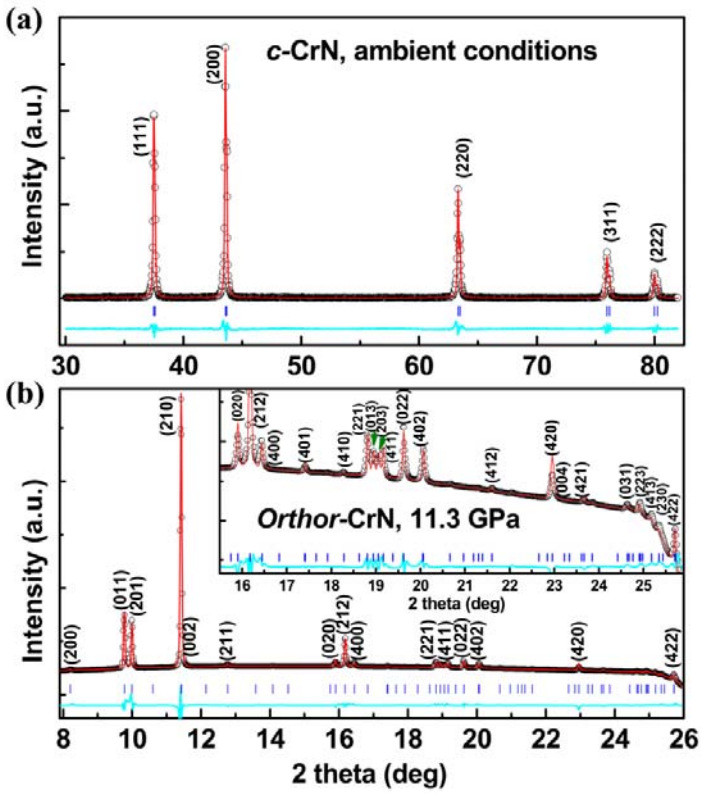
(a)
c-CrN, ambient conditions
Intensity (a.u.)
(111)
(200)
(220)
(311)
(222)
30
40
50
60
70
80
(b)
Orthor-CrN, 11.3 GPa
Intensity (a.u.)
(200)
(011)
(201)
(210)
(002)
(211)
(020)
(212)
(400)
(221)
(411)
(022)
(402)
(420)
(422)
8
10
12
14
16
18
20
22
24
26
2 theta (deg)
16
17
18
19
20
21
22
23
24
25
2 theta (deg)

FIG. 2

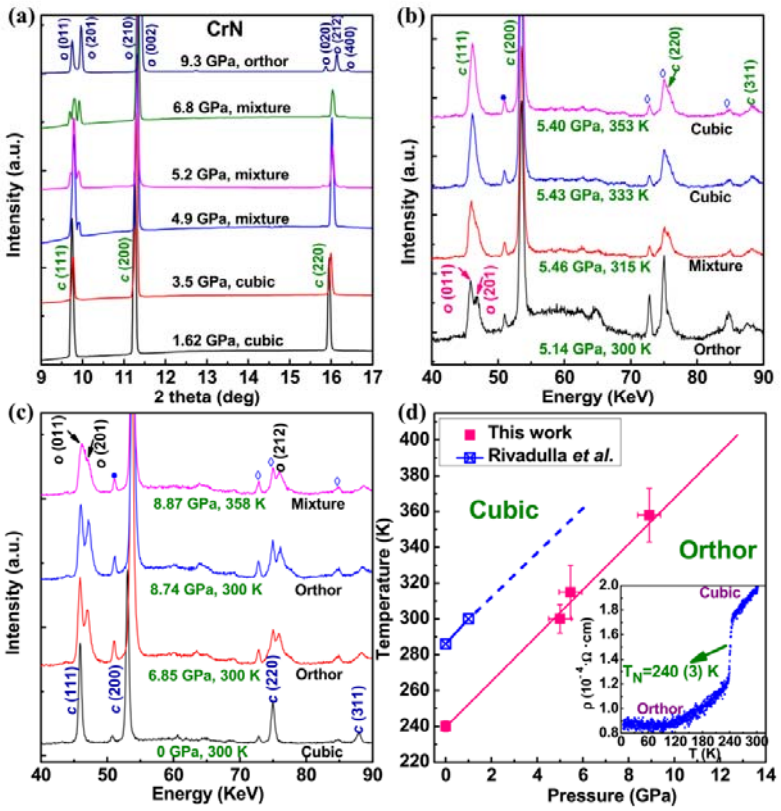
(a)
CrN
9.3 GPa, orthor
6.8 GPa, mixture
5.2 GPa, mixture
4.9 GPa, mixture
3.5 GPa, cubic
1.62 GPa, cubic
o (011)
o (201)
o (210)
o (002)
o (020)
o (212)
o (400)
c (111)
c (200)
c (220)
Intensity (a.u.)
2 theta (deg)
(b)
c (111)
c (200)
c (220)
c (311)
5.40 GPa, 353 K
Cubic
5.43 GPa, 333 K
Cubic
5.46 GPa, 315 K
Mixture
5.14 GPa, 300 K
Orthor
o (011)
o (201)
Intensity (a.u.)
Energy (KeV)
(c)
o (011)
o (201)
o (212)
8.87 GPa, 358 K
Mixture
8.74 GPa, 300 K
Orthor
6.85 GPa, 300 K
Orthor
0 GPa, 300 K
Cubic
c (111)
c (200)
c (220)
c (311)
Intensity (a.u.)
Energy (KeV)
(d)
This work
Rivadulla et al.
Cubic
Orthor
Temperature (K)
Pressure (GPa)
Cubic
Orthor
T_N=240 (3) K
ρ (10^-4 Ω·cm)
T (K)

FIG. 3

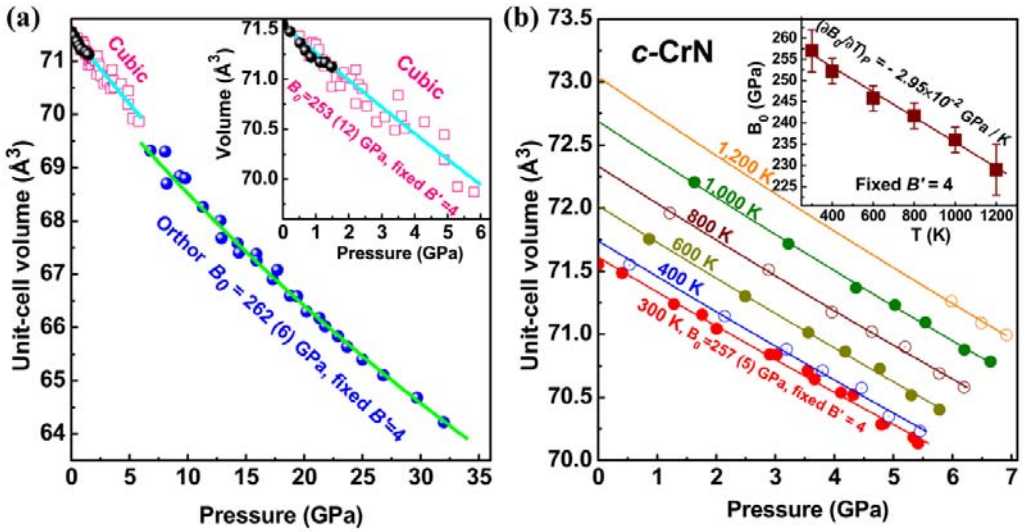
(a)
Cubic
Orthor B_0 = 262 (6) GPa, fixed B'=4
Unit-cell volume (Å^3)
Pressure (GPa)
Volume (Å^3)
Cubic
B_0=253 (12) GPa, fixed B'=4
Pressure (GPa)
(b)
c-CrN
1,200 K
1,000 K
800 K
600 K
400 K
300 K, B_0=257 (5) GPa, fixed B' = 4
Unit-cell volume (Å^3)
Pressure (GPa)
B_0 (GPa)
$(\partial B_0/\partial T)_P$ = - 2.95x10^{-2} GPa / K
Fixed B' = 4
T (K)